Atomic Layer Deposition on Phase-Shift Lithography Generated Photoresist Patterns for 1D Nanochannel Fabrication

Firat Güder,*,† Yang Yang,*,† Michael Krüger,‡ Gregory B. Stevens,‡ and Margit Zacharias†

Nanotechnology Group, Institute of Microsystems Engineering (IMTEK), Albert-Ludwigs-University Freiburg, Georges-Köhler-Allee 103, 79110 Freiburg, Germany, and Freiburger Materialforschungszentrum, Stefan-Meier-Straβe 21, 79104 Freiburg, Germany

ARTICLE

ABSTRACT A versatile, low-cost, and flexible approach is presented for the fabrication of millimeter-long, sub-100 nm wide 1D nanochannels with tunable wall properties (wall thickness and material) over wafer-scale areas on glass, alumina, and silicon surfaces. This approach includes three fabrication steps. First, sub-100 nm photoresist line patterns were generated by near-field contact phase-shift lithography (NFC-PSL) using an inexpensive homemade borosilicate mask (NFC-PSM). Second, various metal oxides were directly coated on the resist patterns with low-temperature atomic layer deposition (ALD). Finally, the remaining photoresist was removed via an acetone dip, and then planar nanochannel arrays were formed on the substrate. In contrast to all the previous fabrication routes, the sub-100 nm photoresist line patterns produced by NFC-PSL are directly employed as a sacrificial layer for the creation of nanochannels. Because both the NFC-PSL and the ALD deposition are highly reproducible processes, the strategy proposed here can be regarded as a general route for nanochannel fabrication in a simplified and reliable manner. In addition, the fabricated nanochannels were used as templates to synthesize various organic and inorganic 1D nanostructures on the substrate surface.

KEYWORDS: ALD • near-field contact phase-shift lithography • nanochannel • nanotemplating • nanowire

1. INTRODUCTION

In the past decade, nanochannels have attracted increasing interest because of their importance in the investigation of fundamental fluidic phenomena (1−5), realization of nanofluidic devices (6−13), and as a platform for template-based nanosynthesis (14−17). Among various strategies, top-down approaches involving bulk/film, surface, and mold micromachining are most widely exploited for achieving orderly and parameter-flexible nanochannel arrays on a large scale (18). The size of the nanochannels generated with these processes depends in one way or another on the patterning technique.

Conventional photolithography presents a fast and effective approach for patterning. However, generating structures in the sub-100 nm regime is still expensive due to resolution enhancing modifications required by the lithography equipment. Serial patterning methods such as electron beam (19) and focused ion beam lithography (20) have also been utilized to generate sub-100 nm structures for nanochannels, but the beam techniques for patterning is often slow and costly. For overcoming the above-mentioned shortcomings, alternative lithographic methods such as nanoimprint, step-and-flash imprint or spacer and interferometric lithography were recently purposed for the fabrication of nanochannels (18, 21) and other in-plane 1D nanostructures (22−24). However, challenges still exist for the ultimate nanochannel fabrication scheme, which should be low-cost, simple (requiring only a few steps to produce channels), and flexible. More importantly, an ideal strategy should also allow fabrication on a variety of base materials with adjustable channel parameters such as channel dimensions, aspect ratio, wall materials and wall thickness, etc.

Here, we present a versatile, low-cost, and flexible approach for the fabrication of millimeter-long, sub-100 nm wide 1D nanochannels with tunable wall properties (wall thickness and material) over wafer-scale areas on glass, alumina, and silicon surfaces. This approach generally includes three fabrication steps, as schematically illustrated in Figure 1a. First, photoresist line patterns are generated by near-field contact phase-shift lithography (NFC-PSL) using a novel borosilicate mask (NFC-PSM). Second, various metal oxides are directly coated on the resist patterns with low-temperature atomic layer deposition (ALD). Finally, the remaining photoresist is removed via an acetone dip, and then planar nanochannel arrays are formed on the substrate. In contrast to all the previously reported fabrication routes, the sub-100 nm photoresist line patterns produced by NFC-PSL are directly employed as sacrificial layers for the creation of nanochannels. As far as we know, this is the first time such a fabrication process is reported in this field. Because both the NFC-PSL and the ALD deposition are highly reproducible processes, the strategy proposed here can be regarded as a general route for nanochannel fabrication in a simplified and reliable manner. Using the nanochannels as

* Corresponding author. E-mail: gueder@imtek.de (F.G.); yang.yang@imtek.de (Y.Y.).
Received for review July 7, 2010 and accepted October 21, 2010
† Institute of Microsystems Engineering.
‡ Freiburger Materialforschungszentrum.
DOI: 10.1021/am100592f
2010 American Chemical Society

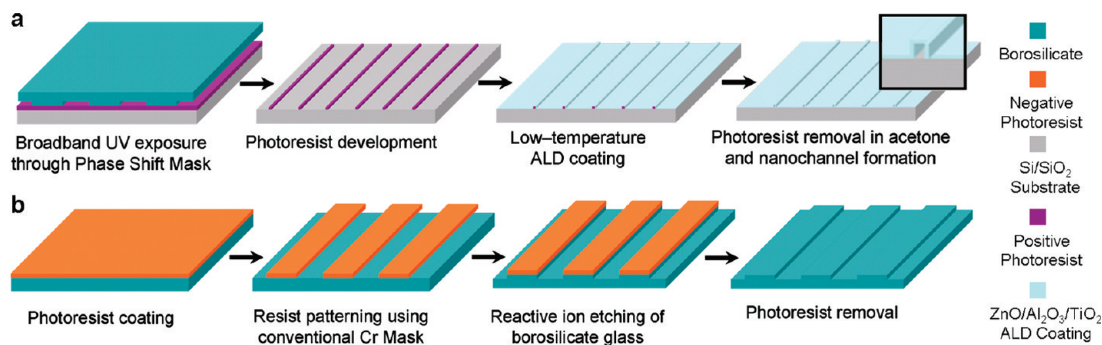

FIGURE 1. Schematic displaying (a) synthesis of low-temperature-ALD-assisted nanochannels and (b) the fabrication procedure of the etched borosilicate near-field contract phase-shift photolithography mask.

templates, we readily generated various organic and inorganic 1D nanostructures as well.

2. EXPERIMENTAL SECTION

2.1. Mask Fabrication. A borosilicate (Schott Borofloat 33) wafer was coated with TSMR-iN027 negative tone photoresist on a spin coater at 1500 rpm (∼400 nm thickness). The photoresist film was exposed (365 nm UV) through a conventional chromium quartz mask containing the grating pattern for 8 s at an exposure dose of 10 mW/cm^2. After exposure, the wafer was postbaked for 90 s at 110 °C and developed in the AZ 726 MIF developer solution for 30 s. The wafer was then etched using CHF_3 (35 sccm)/CF_4 (15 sccm)/Ar (50 sccm) plasma to transfer the resist pattern onto the borosilicate substrate with an etch depth of approximately 330 nm. Finally, the remaining photoresist was stripped by O_2 plasma.

2.2. Photoresist Patterning by NFC-PSM. Glass, silicon, and ALD Al_2O_3-covered silicon wafers were covered with 1.1 μm AZ 5214 (MicroChemicals) image reversal resist by spinning at 6000 rpm. The photoresist film was then exposed through the etched borosilicate mask with broadband UV for 3 s at an exposure dose of 10 mW/cm^2. The borosilicate wafer mask must be in perfect contact with the substrates, and therefore pressure was applied to ensure this before UV exposure. Finally, the photoresist was developed in the AZ 726 MIF developer solution for approximately 1.5 min to wash away the exposed areas leaving behind the sub-100 nm resist lines. Note that the image reversal resist was used in the positive regime, which was achieved by skipping the image reversal procedure after the UV exposure.

2.3. ALD Thin Film Growth. TiO_2/ZnO/Al_2O_3 thin films were grown at 115 °C by reacting titanium isopropoxide, diethylzinc, and trimethylaluminum, respectively, with water vapor in a vertical flow type reactor (OpAL, Oxford Instruments) at pressures between 80 and 180 mTorrs. N_2 was used as the carrier gas with a flow rate of 25 sccm for the ZnO process and 100 sccm for the Al_2O_3 and TiO_2 processes.

2.4. Die Preparation and Channel Formation. Wafers with ALD-coated photoresist structures were sliced into 1 × 1 cm dies and placed in an acetone bath for 12 h to remove the remaining photoresist.

2.5. Characterizations. The high-resolution SEM images and energy-dispersive X-ray (EDX) spectroscopy data were obtained using a Nova NanoSEM (FEI) SEM with a built-in EDX (EDAX) setup. The UV fluorescent microscopy images were acquired using a Leica DMI6000B inverted microscope with a broadband mercury UV light source.

3. RESULTS AND DISCUSSION

3.1. Fabrication and Application of Borosilicate NFC-PSMs for Patterned Photoresist. The NFC-PSMs are fully transparent photomasks which include periodic rectangular trenches on the mask surface with a depth d

$$d = \frac{\lambda}{2(n-1)} \tag{1}$$

where λ is the wavelength of the UV light source and n is an integer. The phase-shifted light at the step edges causes constructive and destructive interference forming dark and bright regions in the intensity profile. These regions are then used to expose a photoresist film, creating line and trench patterns. Detailed working principles, modeling and applications of NFC-PSMs have already been discussed elsewhere (25−28). As opposed to its elastomeric PDMS-based counterparts (29), the borosilicate NFC-PSMs used in our research are not produced through a molding process. Instead, they are directly patterned using conventional lithography and reactive ion etching (RIE) avoiding extra processing for the fabrication of mold masters (see the Supporting Information, Figure S1). Figure 1b displays a schematic visualization of the fabrication process. Due to the hard, glassy nature of the borosilicate, the fabricated masks can be used for an extended period of time. This property of the masks also allows lithographic alignment between the mask and substrate, enabling precise multilayer pattern transfer. As compared to its quartz counterparts (28, 30), borosilicate NFC-PSMs are approximately 10-folds cheaper. Low-cost silicon nitride membrane NFC-PSMs have also been reported for generating sub-100 nm resists patterns. However, these masks require dangerous chemicals for etching the silicon nitride film and are very hard to handle due to the fragile nature of the fabricated masks, which are only 1 μm thick (31). Thus, borosilicate NFC-PSMs provide an excellent alternative for generating nanometer-scale resist patterns.

Panels a and b in Figure 2 exhibit photoresist line patterns produced in our experiments using a homemade borosilicate NFC-PSM. The resist lines are several millimeters long and very uniform over a large area. The interspacing between the lines can be conveniently adjusted by changing the step width of the etched borosilicate mask. The resist lines have a high-aspect-ratio cross-sectional profile with a triangular shape, which is caused by the intensity profile generated by the borosilicate mask during UV exposure. The height of the resist structures can be decreased by using a thinner pho-

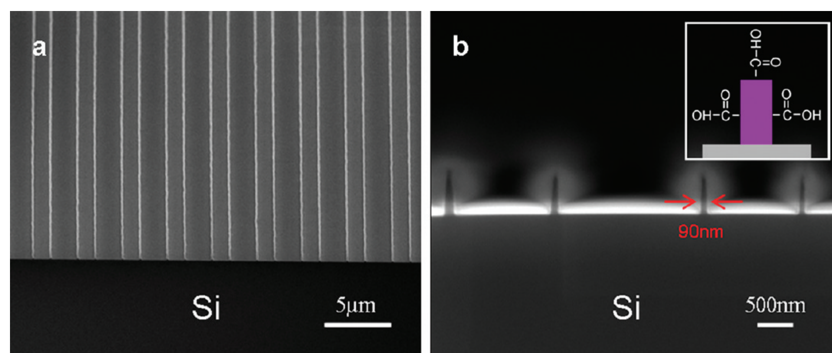

FIGURE 2. SEM images of photoresist structures produced by the borosilicate near-field contact phase-shift lithography mask for a (a) 45° tilted overview, and a (b) cross-sectional view and inset showing surface groups of the developed photoresist.

toresist film, providing a degree of freedom for adjusting the volume of the final nanochannels.

3.2. Low-Temperature ALD and Nanochannel Fabrication. Subsequently, we performed low-temperature ALD of various metal oxides using the prepared photoresist line patterns as a template. In conventional surface micromachining-based inorganic microchannel and nanochannel fabrication, the use of photoresist films as a sacrificial layer is very limited because of their chemical and physical instability. This is because most classical chemical vapor deposition (CVD) techniques used in channel fabrication either require high temperatures for processing or are not able to deposit high-quality (i.e., smooth, powder, and pinhole free), conformal thin films at lower temperatures. The only work coupling photoresist cores and CVD techniques, to the best of our knowledge, was reported by Peeni et al., where an aluminum/photoresist hybrid sacrificial core with a width of, 10 μm, was coated with plasma-enhanced CVD-(PECVD) grown thin films (SiO_2, Si_3N_4, α-Si), and the sacrificial core was later removed via a two-stage etching process creating inorganic nanochannel structures (32). Part of the limitations of classical CVD processes can be overcome by the ALD technique. A unique feature of ALD is that the reactive gases are released into the reactor separately in an alternating, self-limiting manner. Therefore, the ALD method allows deposition of a large selection of high-quality and conformal binary oxide, sulfide, and many other thin films, even at relatively low temperatures (33−36). For instance, ZnO, Al_2O_3, and TiO_2 thin films have already been grown at temperatures as low as 85, 25, and 35 °C, respectively, using the low-temperature ALD technique. Luo et al. once used a low-temperature ALD process to coat photoresist patterns with an Al_2O_3 thin film at 120 °C for the fabrication of 100-nm magnetic nanorings (37). Ye et al. reported a similar ALD process operating at 25 °C to fabricate GaAs metal-oxide-semiconductor structures with comparable dimensions (36). As the dimension of photoresist patterns reduced to sub-100 nm dimensions, their degradation and possible shape change become more sensitive to temperature. Thus, the employment of a suitable deposition temperature is the most crucial point for a conformal coating on photoresist patterns. The AZ 5214 E photoresist used in our experiments is a very suitable resist for the low-temperature ALD process as it is stable at deposition temperatures around 115 °C. Also, when it is used in the positive regime, the hydrophilic surface groups (see inset of Figure 2b) will prevent subsurface nucleation and accordingly allow deposition of smooth and conformal films.

Figure 3a shows a scanning electron microscope (SEM) image of 35 nm TiO_2-coated photoresist lines using the ALD process at 115 °C. As can be seen in the image, the photoresist structures preserve their original triangular shape and have smooth sidewalls. The coated photoresist structures were turned into nanochannels by dipping the TiO_2 coated structures in acetone for approximately 12 h to remove the sacrificial cores (Figure 3b,c). The use of acetone for dissolving the photoresist core eliminates the need for hazardous acids that are often used to remove sacrificial layers. Small acetone molecules easily penetrate into the nanochannels from the open ends and dissolve the resist very effectively, minimizing the time required for the formation of channel structures.

One of the unique properties of ALD is its ability to deposit conformal coatings on ultrahigh-aspect-ratio nanostructures. Elam et al. demonstrated conformal deposition of Al_2O_3 and ZnO thin films on anodic alumina membranes with an aspect ratio of length/diameter up to 10^3 (38). Exploiting this property of ALD, an additional 12 nm of TiO_2 was deposited on the previously fabricated nanochannels. Figure 3d shows the same nanochannel before (left) and after (right) post deposition. The fabricated nanochannel originally had a width of roughly 78 nm, and after the post deposition the width was reduced to 54 nm. Using this method, nanochannels sizes can easily be scaled down to the range 10−20 nm. Therefore, once the initial nanochannels are fabricated by a post ALD deposition, the channel dimensions can be further tuned to desired dimensions, which is a challenge with other fabrication techniques. Please note that the post-ALD coating of the inner channel walls is limited by the diffusion of the reactive species into the channels, which requires long enough exposure times and high enough gas partial pressures to ensure conformal and even film deposition. If these conditions are not satisfied, a tapered channel profile is expected. However, regardless of the inner channel profiles, tuning the size of the channel openings can still be very useful, especially in the size-dependent sieving and separation applications.

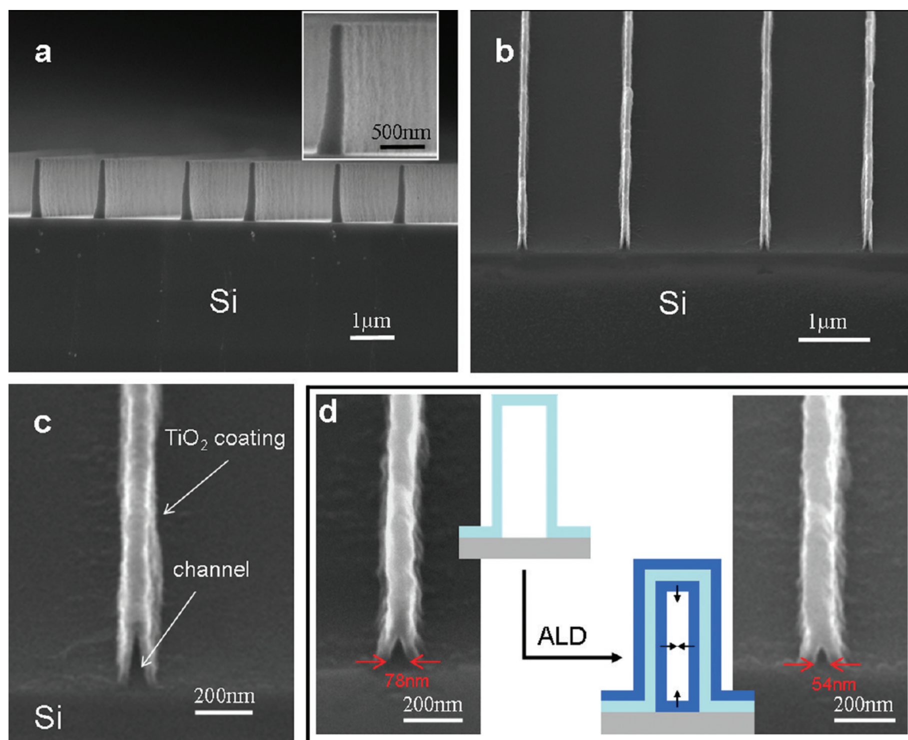

FIGURE 3. SEM images of (a) photoresist structures coated by a 35 nm ALD TiO_2 thin film, (b) a 45° tilted view of TiO_2 nanochannels, (c) a magnified view of b, and (d) a nanochannel before (left) and after (right) post-ALD deposition to scale down the channel dimensions.

A vast number of ALD processes are available for the fabrication of nanochannels composed of materials with various intrinsic wetting, electrical, optical, and thermal properties. In addition to TiO_2, we also successfully deposited Al_2O_3, ZnO, and their hybrid composite thin films on the generated sub-100 nm photoresist patterns by low-temperature ALD for achieving different nanochannels. Furthermore, the ALD technique works equally well for the deposition of composite films even for channels with micrometer dimensions. As an example, 1.2-μm-wide and 500-nm-high photoresist lines produced by conventional lithography were coated with an Al_2O_3/ZnO composite which consisted of a 20 nm Al_2O_3 and a 20 nm ZnO films. The resulting microchannel structures, after the resist removal step, are shown in Figure S2 (Supporting Information). Additionally, very often the nanofluidic systems require microfluidic interfaces to the outside world. The fact that the ALD technique is suitable for the whole dimension range from micrometers to nanometers makes this process very attractive.

3.3. Applications of Nanochannels to Nanotemplating. On the basis of these size-tunable dense nanochannel arrays, facilitated fabrication of complicated nanofluidic devices and bioanalysis can be achieved. In addition, these nanochannels, on substrate, can be used as a template for the fabrication of various kinds of in-plane 1D nanostructures with lengths in millimeters (17, 39−41). We first used the nanochannels consisting of Al_2O_3/ZnO composite walls on a glass substrate and filled them with a green fluorescent protein (GFP) aqueous solution via capillary filling. These channels, with hydrophilic surfaces, were efficiently filled without further assistance as the capillary pressure can locally reach values between 10−100 bar at the nanoscale (21). The GFP-filled channels were clearly observed through their fluorescence emission under an optical microscope when illuminated by mercury UV light (Figure 4a). The green luminance shows a uniform contrast up to a hundred micrometers, confirming that the filling of the GFP is well-proportioned in the continuous nanochannels. This nanochannel-based templating process indeed provides a useful approach to fabricate in-plane inorganic/organic nanocables (oxides/proteins in this case) on a substrate surface. It should be pointed out that since the channels were filled from the right-hand side of the prepared die, some broken nanochannels failed to transport the filled fluid (Figure 4a). Collapsing of the channel walls could be prevented by applying a thicker ALD coating, which would make them more durable to external and intrinsic mechanical stress.

The nanochannels prepared by this method were also used as nanoreactors for the synthesis of metal/semiconductor nanostructures. We used TiO_2 nanochannels fabricated on a 50 nm Al_2O_3-covered Si substrate in these experiments. Similar to the GFP filling mentioned above, a dilute silver nitrate ($AgNO_3$) solution was first placed into the TiO_2 nanochannels by capillary filling. After irradiation with broadband mercury UV for approximately 10 min, silver crystals were formed from the solution inside the channels, resulting in a metallic core. Formation of the metallic crystals upon UV exposure is caused by the well-known photoreduction process of metallic salts (42). A cross-sectional SEM image of the fabricated structure is shown in Figure 4b, where the formation of a planar Ag/TiO_2 core−shell triangular structure can be confirmed (see the Supporting Information, Figure S3: EDX and X-ray photo-

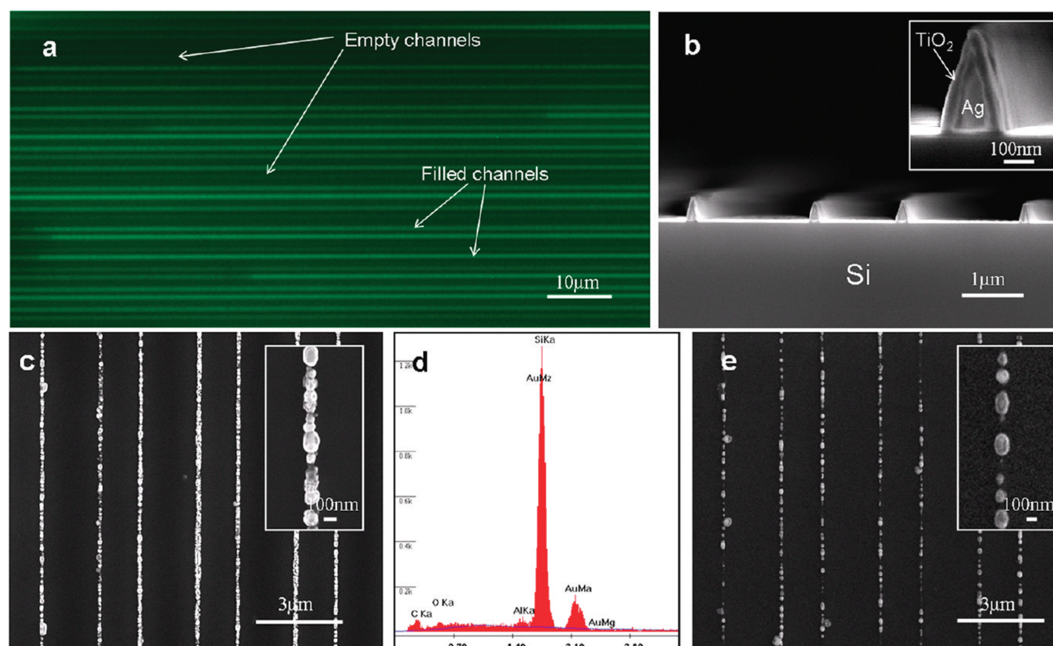

FIGURE 4. (a) UV fluorescent optical image of GFP-filled Al_2O_3/ZnO nanochannels fabricated on a glass substrate, SEM images of (b) Ag/TiO_2 core−shell nanostructures, (c) polycrystalline gold nanowires produced by forming gold crystals inside the nanochannels and stripping the TiO_2 channel cover; (e) gold nanodot arrays produced by annealing the polycrystalline gold nanowires inside the nanochannels and stripping the TiO_2 channel cover, and (d) EDX spectrum when the electron beam is incident on a gold nanowire in c. Note that during the removal of TiO_2, an etch stop layer such as Al_2O_3 is necessary to prevent removal of the nanowires from the Si surface because fluorine-based chemistries readily etch Si.

electron spectrometer (XPS) analyses on the channel cross-section). Because of the spatial confinement of the nanoreactor, the photoreduction reaction only took place in the nanochannels, which accordingly confined the diameter of the formed silver nanowires within the channel size. By changing the concentration of the dissolved silver salt solution, packing of Ag crystallites inside the channel can also be tuned; higher concentrations yield more densely packed and lower concentration less densely packed polycrystalline Ag lines.

By following the same fabrication strategy, Au/TiO_2 core−shell structures were also successfully fabricated using chloroauric acid ($HAuCl_4$) as the precursor. For achieving uncoated gold nanowire arrays arranged on the surface, the TiO_2 channel covers were removed via a CF_4/CHF_3-based RIE process (43), leaving only polycrystalline Au nanowires arranged on the Al_2O_3 surface (Figure 4c). The EDX analysis in Figure 4d and the XPS result (see the Supporting Information, Figure S3) show that the fabricated lines consist purely of elemental Au after the removal of the nanochannels. For this system, the addition of a 2-h annealing step at 550 °C preceding the removal of the TiO_2 cover resulted in disconnected Au nanodot chains instead of long polycrystalline Au nanowires on the surface (Figure 4e). This result is most possibly attributed to annealing-induced partial evaporation of gold along with Ostwald ripening.

As for the future work, the presented technique's ability to produce planar nanochannels can be exploited to produce more complicated templates which allow the fabrication of complex nanostructure designs. Patterned nanostructures may find abundant applications in growth, catalysis, sensing, and conduction. For example, arranged arrays of linear Au dots are promising as catalysts for the site-preferential growth of epitaxial nanowires (44). Moreover, the nanochannel fabrication scheme can be further developed to generate complex micro/nanofluidic device layouts by modifying the borosilicate mask. To generate nanopatterns, the etched side of the near field mask must be in contact with the photoresist. However, patterns with dimensions in the range of several tens of micrometers can be placed on the top side of the mask via structuring a chromium film to define optically dark regions, thus creating a hybrid, all-in-one, double-sided low-cost mask for nano/microfluidic applications in one package (see the Supporting Information, Figure S4).

4. CONCLUSIONS

In summary, a three-step wafer-scale fabrication process producing millimeter-long nanochannels based on the combination of the borosilicate near-field contact phase-shift lithography mask with low-temperature atomic layer deposition was presented. The novel combination of these two processes allows simple, low-cost, and flexible fabrication of nanochannels made of various inorganic materials. The fabricated channels were then used as a physical template to synthesize a number of nanostructures (core−shell, metallic nanowire, and ordered nanodot structures) on the substrate surface. Possible synthesized structures are not limited to the ones presented here and can be extended to other material systems.

Acknowledgment. We thank the IMTEK clean-room staff as well as Kittitat Subannajui and Björn Albrecht for their assistance in the preparation of the experiments and the

development of the mask. We also thank Daniela Mössner for the XPS measurements. This work was supported by Deutsche Forschungsgemeinschaft (DFG) under Contract Za 191/23-1.

Supporting Information Available: SEM images of an etched borosilicate near-field contact phase-shift lithography mask, micrometer-scale Al_2O_3/ZnO nanochannels fabricated on a Si substrate using conventional lithography, EDX and XPS spectra obtained from the Ag/TiO_2 core–shell nanostructure, XPS spectrum obtained from the Au nanostructure, and future prospects for a double-sided hybrid NFC-PSM for all-in-one micro/nanofluidics applications (PDF). This material is available free of charge via the Internet at http://pubs.acs.org.

REFERENCES AND NOTES

(1) Sparreboom, W.; Van Den Berg, A.; Eijkel, J. C. T. *Nat. Nanotechnol.* **2009**, *4*, 713.
(2) Daiguji, H. *Chem. Soc. Rev.* **2010**, *39*, 901.
(3) Rauscher, M.; Dietrich, S. *Ann. Rev. Mater. Sci.* **2008**, *38*, 143.
(4) Schoch, R.; Han, J.; Renaud, P. *Rev. Mod. Phys.* **2008**, *80*, 839.
(5) Tas, N.; Escalante, M.; van Honschoten, J.; Jansen, H.; Elwenspoek, M. *Langmuir* **2010**, *26*, 1473.
(6) Kim, S.; Ko, S.; Kang, K.; Han, J. *Nat. Nanotechnol.* **2010**, *5*, 297.
(7) Jin, X.; Joseph, S.; Gatimu, E.; Bohn, P.; Aluru, N. *Langmuir* **2007**, *23*, 13209.
(8) Lesinski, G.; Sharma, S.; Varker, K.; Sinha, P.; Ferrari, M.; Carson, W. *Biomed. Microdevices* **2005**, *7*, 71.
(9) Han, J.; Craighead, H. *Science* **2000**, *288*, 1026.
(10) Han, A.; Rooij, N.; Staufer, U. *Nanotechnology* **2006**, *17*, 2498.
(11) Wang, M.; Jing, N.; Chou, I.; Cote, G.; Kameoka, J. *Lab Chip* **2007**, *7*, 630.
(12) Daiguji, H.; Oka, Y.; Shirono, K. *Nano Lett.* **2005**, *5*, 2274.
(13) Vlassiouk, I.; Kozel, T.; Siwy, Z. *J. Am. Chem. Soc.* **2009**, *131*, 8211.
(14) Li, J.; Papadopoulos, C.; Xu, J.; Moskovits, M. *Appl. Phys. Lett.* **1999**, *75*, 367.
(15) Huczko, A. *Appl. Phys. Mater. Sci. Process.* **2000**, *70*, 365.
(16) Cao, G.; Liu, D. *Adv. Colloid Interface Sci.* **2008**, *136*, 45.
(17) Lu, N.; Chen, X.; Molenda, D.; Naber, A.; Fuchs, H.; Talapin, D. V.; Weller, H.; Müller, J.; Lupton, J. M.; Feldmann, J.; Rogach, A. L.; Chi, L. *Nano Lett.* **2004**, *5*, 885.
(18) Mijatovic, D.; Eijkel, J. C. T.; van den Berg, A. *Lab Chip* **2005**, *5*, 492.
(19) Choi, S.; Yan, M.; Adesida, I. *Appl. Phys. Lett.* **2008**, *93*, 163113.
(20) Campbell, L.; Wilkinson, M.; Manz, A.; Camilleri, P.; Humphreys, C. *Lab Chip* **2004**, *4*, 225.
(21) Abgrall, P.; Nguyen, N. T. *Anal. Chem.* **2008**, *80*, 2326.
(22) Li, H. W.; Huck, W. T. S. *Nano Lett.* **2004**, *4*, 1633.
(23) Kim, M.; Kang, B.; Yang, S.; Drew, C.; Samuelson, L. A.; Kumar, J. *Adv. Mater.* **2006**, *18*, 1622.
(24) Guo, L. J. *Adv. Mater.* **2007**, *19*, 495.
(25) Moreau, W. M. *Semiconductor Lithography: Principles and Materials*; Plenum: New York, 1988.
(26) Xia, Y. N.; Rogers, J. A.; Paul, K. E.; Whitesides, G. M. *Chem. Rev.* **1999**, *99*, 1823.
(27) Chen, Y.; Pepin, A. *Electrophoresis* **2001**, *22*, 187.
(28) Wang, F.; Weaver, K.; Lakhtakia, A.; Horn, M. *Optik* **2005**, *116*, 1.
(29) Rogers, J.; Paul, K.; Jackman, R.; Whitesides, G. *Appl. Phys. Lett.* **1997**, *70*, 2658.
(30) Fritze, M.; Tyrrell, B. M.; Astolfi, D. K.; Lambert, R. D.; Yost, D. W.; Forte, A. R.; Cann, S. G.; Wheeler, B. D. *Lincoln Lab. J* **2003**, *14*, 237.
(31) Alkaisi, M.; Blaikie, R.; McNab, S. *J. Vac. Sci. Technol., B* **1998**, *16*, 3929.
(32) Peeni, B.; Conkey, D.; Barber, J.; Kelly, R.; Lee, M.; Woolley, A.; Hawkins, A. *Lab Chip* **2005**, *5*, 501.
(33) Puurunen, R. *J. Appl. Phys.* **2005**, *97*, 121301.
(34) Kim, H. *J. Vac. Sci. Technol., B* **2003**, *21*, 2231.
(35) Knez, M.; Nielsch, K.; Niinistö, L. *Adv. Mater.* **2007**, *19*, 3425.
(36) Ye, P.; Wilk, G.; Tois, E.; Wang, J. *Appl. Phys. Lett.* **2005**, *87*, 013501.
(37) Luo, Y.; Du, Y.; Misra, V. *Nanotechnology* **2008**, *19*, 265301.
(38) Elam, J.; Routkevitch, D.; Mardilovich, P.; George, S. *Chem. Mater.* **2003**, *15*, 3507.
(39) Zhang, M. Z.; Lenhert, S.; Wang, M.; Chi, L. F.; Lu, N.; Fuchs, H.; Ming, N. B. *Adv. Mater.* **2004**, *16*, 409.
(40) Guo, L. J.; Cheng, X.; Chou, C. F. *Nano Lett.* **2004**, *4*, 69.
(41) Zhang, B.; Wenig, Y. Y.; Huang, X. P.; Wang, M.; Peng, R. W.; Ming, N. B.; Yang, B. J.; Lu, N.; Chi, L. F. *Adv. Mater.* **2009**, *21*, 3576.
(42) Kurihara, K.; Kizling, J.; Stenius, P.; Fendler, J. H. *J. Am. Chem. Soc.* **1983**, *105*, 2574.
(43) Dekker, J.; Kolari, K.; Puurunen, R. L. *J. Vac. Sci. Technol., B* **2006**, *24*, 2350.
(44) Fan, H. J.; Werner, P.; Zacharias, M. *Small* **2006**, *2*, 700.

AM100592F